NANOSYSTEMS: PHYSICS, CHEMISTRY, MATHEMATICS, 2014, 5 (4), P. 564–573

EFFECT OF HIGH PRESSURES AND HIGH TEMPERATURES ON STRUCTURAL AND MAGNETIC CHARACTERISTICS OF NANOSTRUCTURED SOLID SOLUTIONS $Zn_{1-x}Fe_xO$

T. V. Dyachkova[1], V. N. Krasil'nikov[1], O. I. Gyrdasova[1], E. V. Shalaeva[1], A. P. Tyutyunnik[1], V. V. Marchenkov[2], Yu. G. Zaynulin[1], H. W. Weber[3]

[1]Federal State government-financed research institution Institute of Solid State Chemistry of the Ural Branch of the Russian Academy of Sciences, Ekaterinburg , Russia

[2]Federal State government-financed research institution Institute of Metal Physics of the Ural Branch of the Russian Academy of Sciences, Ekaterinburg, Russia

[3]Atominstitut, Vienna University of Technology, Vienna, Austria

dyachkova@ihim.uran.ru, kras@ihim.uran.ru, gyrdasova@ihim.uran.ru, shalaeva@ihim.uran.ru, tyutyunnik@ihim.uran.ru, march@imp.uran.ru, zaynulin@ihim.uran.ru, weber@ati143.ac.at

PACS 71.20.Nr, 73.63.Bd, 75.50.Pp

Nanostructured solid solutions of the composition $Zn_{1-x}Fe_xO$ ($0 \leqslant x \leqslant 0.075$) with tubular aggregate morphology, synthesized by the precursor method, were subjected to thermobaric treatment at P = 5 GPa and T = 600–700°C. Using the samples with $x = 0.05$ as an example, it was shown that the application of pressure leads to morphology variation, reduction of structural parameters and to an increase in ferromagnetism.

Keywords: High pressure - high temperature, nanomaterials, glycolate, semiconductors.

Received: 16 June 2014
Revised: 30 June 2014

1. Introduction

Increased interest in zinc oxide, doped with cations of ferromagnetic metals, such as manganese, iron, cobalt and nickel, is due to the need to find new magnetic materials for spintronics that open up possibilities of developing magnetoresistive memory cells, spin light-emitting diodes and field-effect transistor, as well as magnetic field sensors and quantum computer components [1–3]. Although such materials as solid solutions $Zn_{1-x}M_xO$ contain only several atomic percents of magnetic impurities with negligibly small exchange interaction between them, ferromagnetism can occur in them even at room temperature. The magnetically ordered state observed for low-dimensional forms of zinc oxide, for example, nanopowders and thin films, consists not only in a greater degree of imperfection of such structures as compared with bulk objects, but also in the appearance of quantum-dimensional effects that manifest themselves during the transition into the nanodimensional state [2, 4–11]. The unique combination of semiconducting and ferromagnetic properties of the solid solutions $Zn_{1-x}Fe_xO$ makes them promising materials for practical application in the development of devices based on the spin-dependent transport effect and attracts the attention of a wide range of specialists including those concerned in synthesis of nanomaterials, whose efforts are directed at the elaboration of new methods for synthesis of samples with preassigned composition that provide the possibility to control the degree of dispersity and structure imperfection and to affect their magnetic properties [7–11].

Among the methods of synthesis of room-temperature ferromagnetics based on iron-doped zinc oxide described in the literature, the most widespread techniques are solid-phase synthesis [12, 13], self-propagating high-temperature synthesis [14, 15], solvothermal synthesis [11, 16], sol-gel synthesis [17, 18] and synthesis by deposition from aqueous solution in the form of hydroxides [19, 20]. A method for the production of polycrystalline ferromagnetic samples of the composition $Zn_{0.99}Fe_{0.01}O$ from mixtures of ZnO and Fe_3O_4 oxides by the solid-phase reaction technique combined with high-temperature treatment (2 and 5 GPa) has been reported previously [21].

The problem of synthesizing nanostructured iron-doped zinc oxide with a high degree of dispersity and intrinsic imperfection can be solved via the precursor method, the most important advantage of which is the possibility of dosed replacement of zinc by a magnetic metal in the precursor matrix. Thermal treatment of precursor under selected conditions allows the synthesis of oxides with a preset composition and expected morphological and dimensional aggregate parameters. So, as a result of heating in air at temperatures above 400°C, the octahedral crystals of $Zn_{1-x}Fe_x(OCH_2CH_2O)$ glycolate undergo a pseudomorphous transformation into octahedral aggregates of the oxide $Zn_{1-x}Fe_xO$, while extended crystals of formate glycolate $Zn_{1-x}Fe_x(HCOO)(OCH_2CH_2O)_{1/2}$ – into oxide nanotubes with diameters of 150–300 nm consisting of 10–15 nm crystallites [22].

The aim of this work was to examine the effect of annealing temperature and pressure on the structural and magnetic properties of nanodispersed solid solutions $Zn_{1-x}Fe_xO$ with tubular aggregates. In the synthesis of the samples, the advantages of the precursor method were combined with the advantages of thermobaric treatment. Nanotubular samples of the composition $Zn_{0.95}Fe_{0.05}O$, preliminarily synthesized by the precursor technique [22], were treated at quasi-hydrostatic pressure (5 GPa) at a temperature of 600–700°C; after that, their phase composition, microstructure and magnetic characteristics were studied.

2. Experiment technique

For the production of nanostructured iron-doped zinc oxide with tubular aggregate morphology, we employed the precursor method; the precursor was the formate glycolate of the composition $Zn_{1-x}Fe_x(HCOO)(OCH_2CH_2O)_{1/2}$, which was synthesized by the following reaction [22–23]:

$$\begin{gathered} Zn_{1-x}Fe_x(HCOO)_2 \cdot 2H_2O + 1/2HOCH_2CH_2OH = \\ Zn_{1-x}Fe_x(HCOO)(OCH_2CH_2O)_{1/2} + HCOOH\uparrow + 2H_2O \end{gathered} \tag{1}$$

The formate $Zn_{1-x}Fe_x(HCOO)_2{\cdot}2H_2O$ necessary for reaction (1) was synthesized by reaction between dilute formic acid and mixtures of zinc oxide and iron with heating:

$$(1-x)ZnO + xFe + 2HCOOH + H_2O = Zn_{1-x}Fe_x(HCOO)_2 \cdot 2H_2O + xH_2\uparrow \tag{2}$$

Using microscopic analysis, it was found that formate glycolate $Zn_{1-x}Fe_x(HCOO)(OCH_2CH_2O)_{1/2}$ is isolated from the solution in ethylene glycol in the form of fibrous or needle-shaped crystals (reaction 1) upon exposure at 120°C for 2 h. The degree of substitution of iron for zinc in $Zn_{1-x}Fe_x(HCOO)(OCH_2CH_2O)_{1/2}$ does not exceed 10 at. %. In order to produce solid solution samples of the composition $Zn_{1-x}Fe_xO$ with tubular aggregate morphology, the precursor was heated in air with a rate of 10°C/min up to 500°C, exposed at this temperature for 2 h and cooled to room temperature with the furnace. The synthesized samples in the form of finely-dispersed orange powders that served as precursors were examined using X-ray diffraction analysis and then were subjected to thermobaric treatment. The experiments were carried out on a hydraulic press in a standard toroid-type high-pressure chamber. The powder of the composition $Zn_{0.95}Fe_{0.05}O$ was tamped tightly into a graphite cup that served simultaneously as a heater and then it was placed into a container made of lithographic stone – a natural mineral consisting mainly of calcium carbonate $CaCO_3$. To prevent contamination of the sample with carbon, the inside walls of the heater were isolated with boron nitride. The sample was compressed between the press anvils until the necessary pressure was reached, and after that, the temperature was raised. Upon exposure at a preset temperature, the sample under pressure was quenched by abrupt decrease of temperature. Then the pressure was released and the container with the samples was removed from the press. The experimental conditions and the structural characteristics of the produced preparations are given in Table 1.

TABLE 1. The crystallographic characteristics of the $Zn_{0.95}Fe_{0.05}O$ sample before treatment (1) and after treatment at P = 5 GPa, T = 600°C (2) and P = 5GPa, T = 700°C (3)

Sample No.	a (Å)	c (Å)	P (GPa)	T (°C)	Sp. gr.	Content, weight %	CSR (nm)
1	3.2502	5.2074	–	–	$P6_3mc$	100 m%	46.04
2	3.2509	5.2059	5	600	$P6_3mc$	100 m%	123.61
3	3.2489	5.2034	5	700	$P6_3mc$	84.0 m %	93.83
	3.2690	5.2247			$P6_3mc$	9.4 m %	33.65

The phase analysis of the precursors and the products of their thermolysis was performed be means of a POLAM S–112 polarizing microscope in transmitted light (the refractive indices were determined by the immersion method) and a STADI–P X-ray powder automated diffractometer (STOE, Germany) in $CuK_{\alpha 1}$ radiation using the X-ray diffraction database PDF-2 (Release 2009). Thermogravimetric analysis was carried out on a SETSYS EVOLUTION thermal analyzer (SETARAM, France) at a heating rate of 10°C/min in air. The size and shape of the particles of the thermolysis products were determined by scanning electron microscopy on a JSM JEOL 6390LA device. The structure of the thermolysis products was studied by transmission electron microscopy on a JEM–200 CX microscope. To determine the content of zinc and iron, elemental analysis was performed by the atomic absorption spectroscopy method in acetylene-air flame on a Perkin-Elmer device and by atomic emission method on a JY–48 spectrum analyzer with inductively coupled plasma. The magnetic properties of the synthesized $Zn_{1-x}Fe_xO$ samples were measured in the Atom Institute of the Vienna University of Technology on a MPMS XL7 SQUID magnetometer produced by Quantum Design in magnetic fields to 10 kOe in the temperature range from 4.2 to 330 K, as well as in the Multiple Access Center at the IMP UB RAS on a 7407 VSM vibration magnetometer produced by Lake Shore Cryotronics in magnetic fields to 17 kOe at room temperature.

3. Results and discussion

According to the X-ray phase analysis data, the thermolysis products of the precursor in air are solid solutions of the composition $Zn_{1-x}Fe_xO$ ($0 \leqslant x \leqslant 0.075$) with wurtzite structure

(Fig. 1). Thermal decomposition of formate glycolate $Zn_{1-x}Fe_x(HCOO)(OCH_2CH_2O)_{1/2}$ is an exothermic process, occurring in two stages from ∼280–500°C, which agrees with the presence of two anion types, $HCOO^-$ and $OCH_2CH_2O^{2-}$, in the crystal structure of this compound. The mass loss of the $Zn_{0.95}Fe_{0.05}(HCOO)(OCH_2CH_2O)_{1/2}$ sample determined by thermogravimetric analysis differed insignificantly from that calculated with allowance for its transformation into $Zn_{0.95}Fe_{0.05}O$. The common feature of thermal decomposition of $Zn_{1-x}M_x(HCOO)(OCH_2CH_2O)_{1/2}$ (M = V, Cr, Mn, Fe, Co, Ni, Cu) – the solid solutions, in which d metals substitute for zinc in the $Zn(HCOO)(OCH_2CH_2O)_{1/2}$ structure – is that the fibrous crystals of this substance transform during heating in air into aggregates of $Zn_{1-x}M_xO$ oxide having a tubular structure [22–29]. The size and microstructure of $Zn_{0.95}Fe_{0.05}(HCO)$ tubes depend on the formation conditions of precursor crystals and their heat treatment, as well as on the type and concentration of the dopant. The length of the tubular aggregates $Zn_{1-x}Fe_xO$ can exceed 30 μm and their diameter is 100–300 nm depending on the iron concentration (Fig. 2 a,b). As the concentration of iron increases, the tube walls become thinner and during rapid heating this can lead to their rupture in the direction parallel to their lengthening.

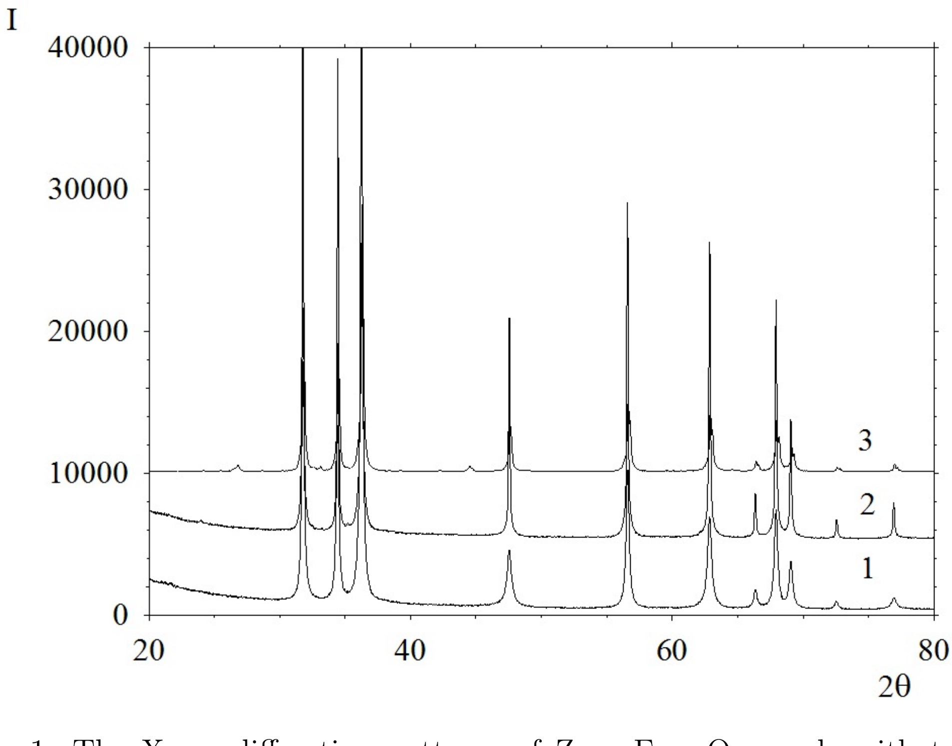

FIG. 1. The X-ray diffraction patterns of $Zn_{0.95}Fe_{0.05}O$ sample with tubular morphology: before treatment (1) and after treatment at P = 5 GPa at T = 600°C (2) and T = 700°C (3)

The bright-field electron-microscope images of $Zn_{0.95}Fe_{0.05}O$ oxide aggregates formed in the thermal decomposition of $Zn_{0.95}Fe_{0.05}(HCOO)(OCH_2CH_2O)_{1/2}$ during heating in air show that they are tubular quasi-one-dimensional structures built of crystallites with an average dimension of ∼10 nm (Fig. 3 a,b). The Debye selected-area diffraction pattern (Fig. 3c) and the dark-field image (Fig. 3d) in $(100)_{ZnO}$, $(002)_{ZnO}$ and $(101)_{ZnO}$ reflections correspond to the polycrystalline nanodispersed structure of quasi-one-dimensional compounds $Zn_{0.95}Fe_{0.05}O$.

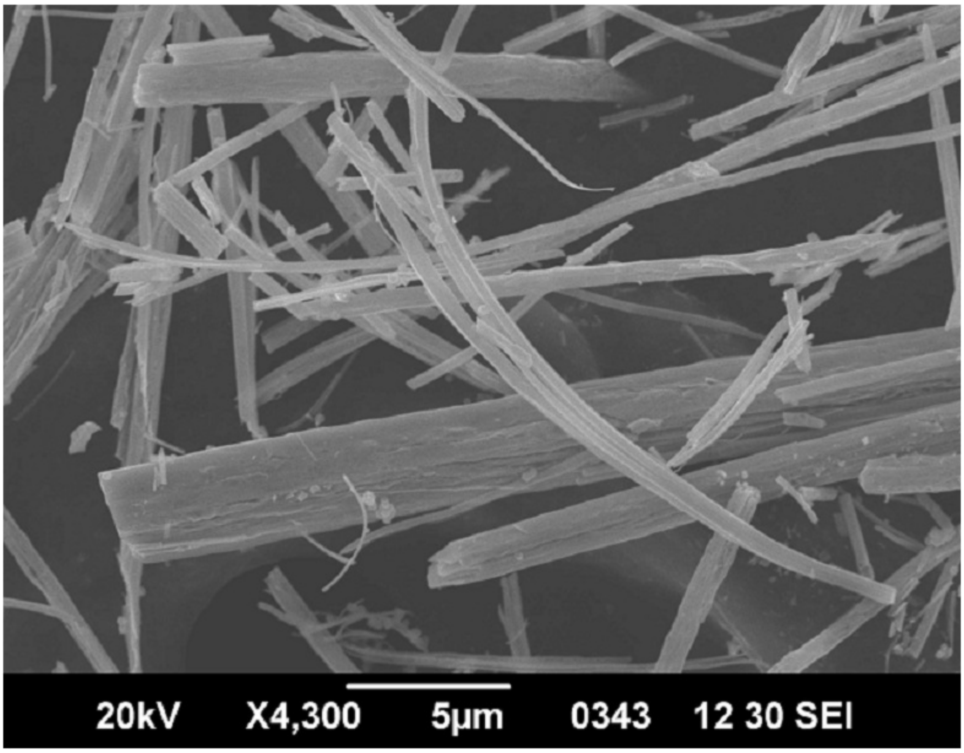

FIG. 2. The XEM image of the sample of the composition $Zn_{0.95}Fe_{0.05}O$ produced by thermolysis of $Zn_{0.95}Fe_{0.05}(HCOO)(OCH_2CH_2O)_{1/2}$ at 500°C in air

The powders of the composition $Zn_{0.95}Fe_{0.05}O$, produced by the precursor method were treated at different pressures (P = 5 – 9 GPa) and temperatures (T = 500, 600, 700, 900°C). The experiments showed that the initial wurtzite ZnO structure (sp. gr. – $P6_3mc$) remains only in a very narrow interval of pressures P = 5 GPa and temperatures T = 600–700°C. Under softer treatment conditions, an impurity phase of the composition $Zn_5(OH)_6(CO_3)_2$ is found, whereas under more rigorous conditions, the high-temperature cubic phase ZnO (sp. gr. – *Fm3m*) and $ZnFe_2O_4$ emerge. As is seen from Fig. 1 and Table 1, the crystal structure typical of the initial sample $Zn_{0.95}Fe_{0.05}O$ with tubular-shaped aggregates (1) remains after thermobaric treatment at 600°C (2). However, the morphology of the samples changes dramatically – the tubular form of the particles transforms into a round shape with lamellar inclusions (Fig. 4a). When the temperature is increased to 700°C (3), two phases with different lattice parameters are formed, one of which is iron-rich (84.0 mass %) and the other, on the contrary, is iron-depleted (9.4 mass %). The shape of the particles becomes more rounded (Fig. 4b). Besides the principal lines belonging to different forms of $Zn_{1-x}Fe_xO$, the X-ray diffraction pattern (Fig. 1) contains lines of boron nitride and graphite (heater material). According to our estimates, the coherent scattering region (CSR) increases with temperature.

Figure 5 presents the magnetization curves at T = 4.2 K (-268.95°C) for $Zn_{0.95}Fe_{0.05}O$ samples 2 and 3 (see Table 1) treated at P = 5 GPa, T = 600°C and T = 700°C. It is seen that a hysteresis loop with coersive force of 165 and 400 Oe is observed for the both samples, respectively. The values of magnetization M estimated in 10 kOe field are M = $9.71\cdot10^{-2}$ emu/g (or $4.1\cdot10^{-2}$ μ_B/Fe) and M = $2.02\cdot10^{-1}$ emu/g (or $8.5\cdot10^{-2}\mu_B$/Fe), respectively. The temperature dependences M(T) in 1000 Oe field displayed in Fig. 6 allow us to suppose that the ferromagnetic state can be observed up to room temperatures at least in sample 3.

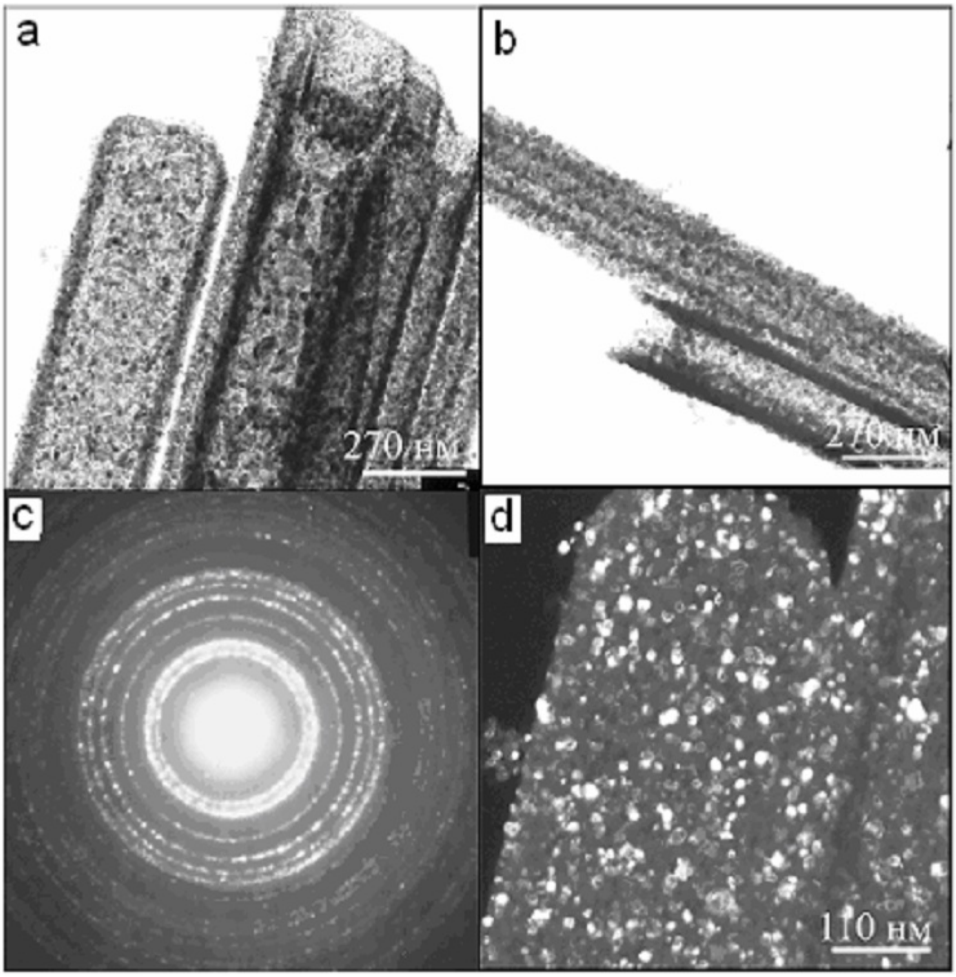

FIG. 3. The bright-field electron-microscope images of quasi-one-dimensional $Zn_{0.95}Fe_{0.05}O$ with tubular morphology (a, b). The Debye selected-area diffraction pattern (c) and the dark-field image (d) in $(100)_{ZnO}$, $(002)_{ZnO}$ and $(101)_{ZnO}$ reflections correspond to the polycrystalline nanodispersed structure of quasi-one-dimensional compounds. The average size of the crystallites is ~10 nm

Therefore the magnetization curves have been measured at T = 290 K (17°C) (Fig. 7). It was found that at room temperature, sample 2 is paramagnetic, i. e. magnetization increases linearly with a stronger magnetic field, while hysteresis is absent. By contrast, for sample 3, a hysteresis loop with coercive force of 100 Oe is observed, and magnetization estimated in 10 kOe field is $M = 8.25 \cdot 10^{-2}$ emu/g (or $3.5 \cdot 10^{-2} \mu_B$/Fe). Thus, it is shown that the increase in the treatment temperature from T = 600°C to T = 700°C results in more than twofold enhancement of magnetization in the region of liquid helium temperatures (transition from sample 2 to sample 3). At room temperature, sample 2 transforms into a paramagnetic state, whereas sample 3 still exhibits ferromagnetic properties. In work [21], investigations have been performed into magnetization of $Zn_{0.99}Fe_{0.01}O$ samples synthesized by annealing of a mixture of ZnO and Fe_3O_4 at P = 0; 2 and 5 GPa and T = 600°C for 30 min, which exhibited ferromagnetism in the temperature range from 5 K (-268°C) to 300 K (27°C). Moreover, the authors [21] also observed that magnetization grows when the pressure is increased during synthesis up to P = 5 GPa at constant temperature T = 600°C. Like in

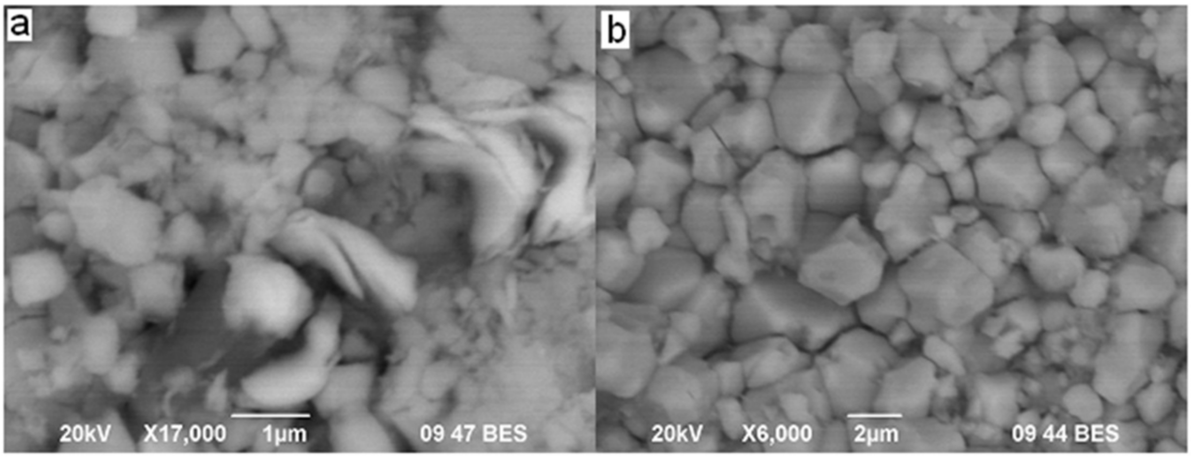

FIG. 4. The XEM images of the particles of the sample with the initial composition $Zn_{0.95}Fe_{0.05}O$ after heating under a pressure of 5 GPa at 600 (a) and 700°C (b)

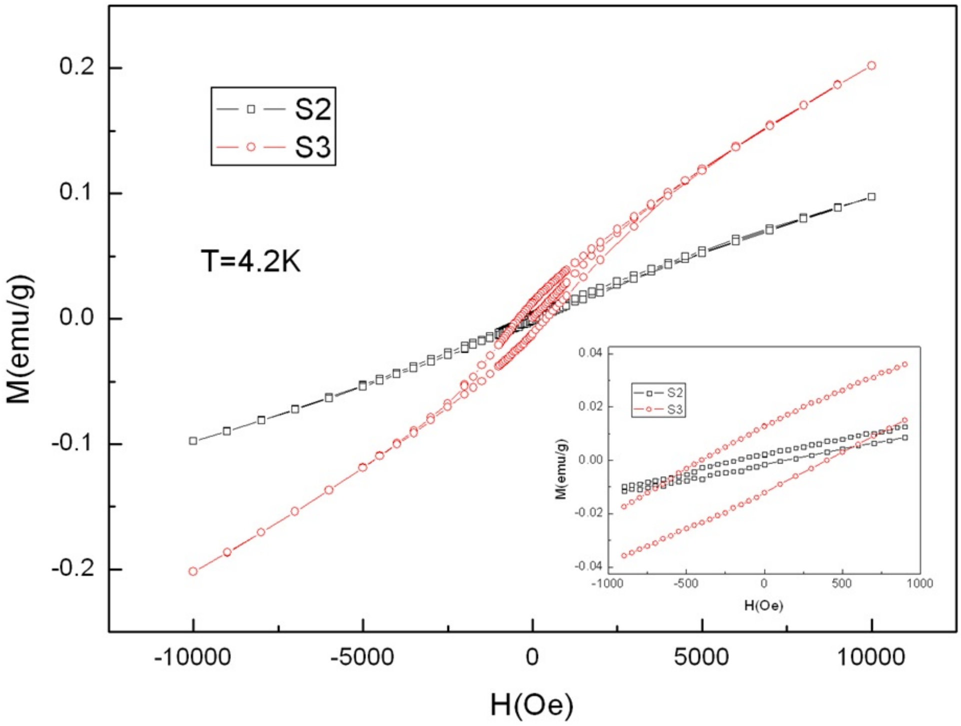

FIG. 5. The magnetizations curves of samples 2 (S2) and 3 (S3) at T = 4.2 K. The hysteresis loops for the both samples are shown in the inset

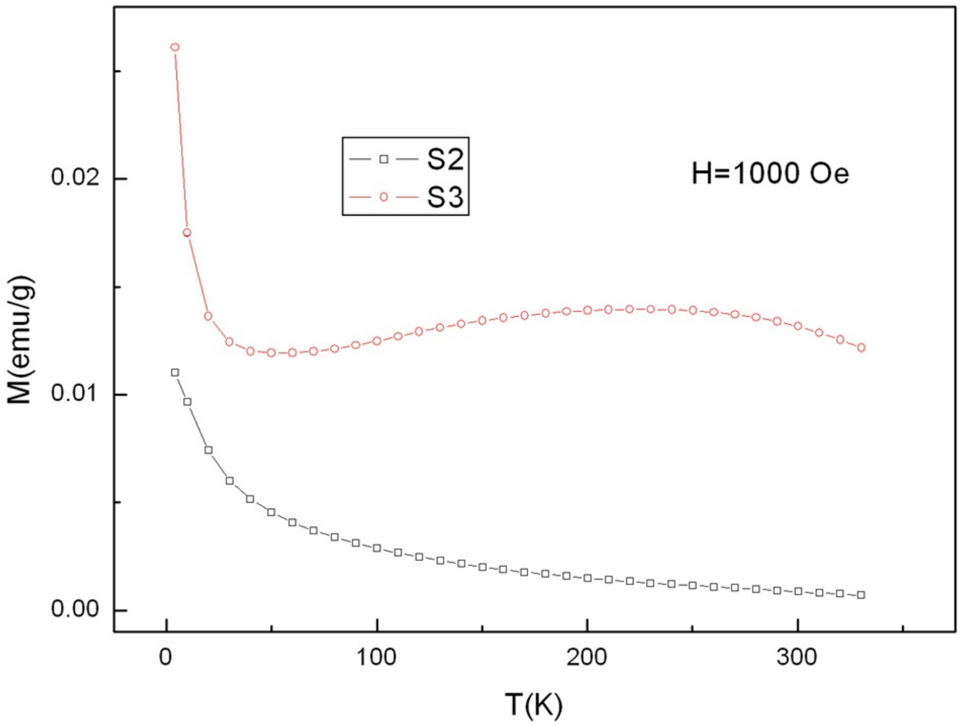

FIG. 6. The temperature dependences of magnetization for samples 2 (S2) and 3 (S3) in 1000 Oe field

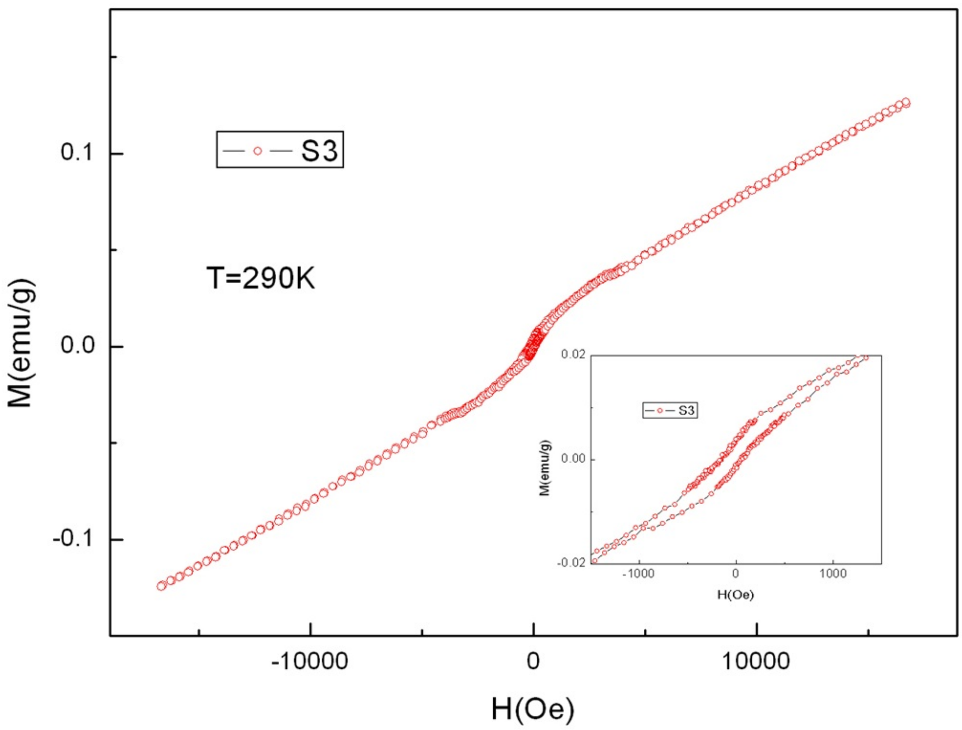

FIG. 7. The magnetizations curves of samples 2 (S2) and 3 (S3) at T = 290 K. The hysteresis loop is shown in the inset

work [21], we obtained comparable magnetization values for iron-doped zinc oxide samples, though their saturation fields are higher.

Thus, in the studies performed, it was established that thermobaric treatment of the oxide of the composition $Zn_{0.95}Fe_{0.05}O$ with tubular-shaped aggregates at T = 600°C and P = 5 GPa leads to the appearance of ferromagnetism and to the transformation of nanotubes into agglomerates having a rounded shape, which is similar to the shape of the particles of room-temperature ferromagnetics produced by solid-phase annealing of ZnO and Fe_3O_4 oxide mixtures under identical conditions [21].

Acknowledgments

The work was supported by the RFBR (grant No. 12-03-00453-) and the Presidium of RAS (project No. 12--3-1009).

References

[1] Cheng H., Cheng J., Zhang Y., Wang Q.-M. Large-scale fabrication of ZnO micro-and nano- structures by microwave thermal evaporation deposition. *Journal of Crystal Growth*, **299**(1), P. 34–40 (2007).

[2] Singh R. Unexpected magnetism in nanomaterials. *Journal of Magnetism and MagneticMaterials*, **346**, P. 58–73 (2013).

[3] Yilmaz C., Unal U. Synthesis and Characterization of Hierarchical ZnO Structures by a Single-Step Electrodeposition under Hydrothermal Conditions. *Electrochimica Acta*, **123**, P. 405–411 (2014).

[4] Murugadoss G. Synthesis and Characterization of Transition Metals Doped ZnO Nanorods. *J. Mater. Sci. Technol.*, **28**(7), P. 587–593 (2012).

[5] Ahmed F., Kumar S., Arshi N., et al. Direct relationship between lattice volume, band gap, morphology and magnetization of transition metals (Cr, Mn and Fe)-doped ZnO nanostructures. *Acta Materialia*, **60**, P. 5190–5196 (2012).

[6] Wibowo J.A., Djaja N.F., Saleh R. Cu- and Ni-Doping Effect on Structure and Magnetic Properties of Fe-Doped ZnO Nanoparticles. *Advances Mater. Phys. Chem.*, **3**, P. 48–57 (2013).

[7] Karmakar D., Dasgupta I., Das G.P., Kawazoe Y. High Temperature Ferromagnetism in Fe-Doped ZnO: a Density Functional Investigation. *Materials Transactions*, **48**(8), P. 2119–2122 (2007).

[8] Samariya A., Sighal R.K., Kumar S., et al. Defect-induced reversible ferromagnetism in Fe-doped ZnO semiconductor: An electronic structure and magnetization study. *Mater. Chem. Phys.*, **123**(2-3), P. 678–684 (2010).

[9] Limaye M.V., Sngh S.B., Das R., et al. Room temperature ferromagnetism in undoped and Fe doped ZnO nanorods: Microwave-assisted synthesis. *J. Solid State Chem.*, **184**, P. 391–400 (2011).

[10] Panigrahy B., ASlam M., Bahadur D. Effect of Fe doping concentration on optical and magnetic properties of ZnO nanorods. *Nanotechnology*, **23**, P. 11601 (2012).

[11] Lokesh R.N., Balakrishnan L., Jeganathan K., et al. Role of surface functionalization in ZnO:Fe nanostructures. *Mater. Sci. Eng. B*, **183**, P. 39–46 (2014).

[12] Colak H., Turkoglu O. Synthesis, Crystal Structural and Electrical Conductivity Properties of Fe-Doped Zinc Oxide Powders at High Temperatures. *J. Mater. Sci Technol*, **28**, P. 268–274 (2012).

[13] Wang F., Huang W.-W., Li S.-Y., et al. The magnetic properties of $Fe_xZn_{1-x}O$ synthesized via the solid-state reaction route: Experiment and theory. *Journal of Magnetism and Magnetic Materials*, **340**, P. 5–9 (2013).

[14] Denisha M.L., Jayanna H.S., Ashoka S., Chndrappa G.T. Temperature dependent electrical conductivity of Fe doped ZnO nanoparticles prepared by solution combustion method. *J. Alloys Compd*, **485**, P. 538–541 (2009).

[15] Dhiman P., Sharma S.K., Knobel M., Ritu R., Singh M. Magnetic Properties of Fe doped ZnO Nanosystems Synthesized by Solution Combustion Method Res. *J. Resent Sci*, **1**(8), P. 48–52 (2012).

[16] Behera A.K, Mohapatra N., Chatterjee S. Effect of Fe Doping on Optical and Magnetic Properties of ZnO Nanorods. *J. Nanosci. Nanotechnol*, **14**(5), P. 3667–3672 (2014).

[17] Wu G.S., Xie T., Yuan X.Y., et al. Controlled synthesis of ZnO nanowires or nanotubes via sol–gel template process. *Solid State Communications*, **134**, P. 485–489 (2005).

[18] Liu H., Yang J., Zhang Y., Yang L., Wei M., Ding X. Structure and magnetic properties of Fe-doped ZnO prepared by the sol–gel method. *J. Phys.: Condens. Mater.*, **21**, P. 145803 (2009).

[19] Zhang H.-W., Wei Z.-R., Li Z.-Q., Dong G.-Y. Room-temperature ferromagnetism in Fe-doped, Fe- and Cu-codoped ZnO diluted magnetic semiconductor. *Materials Letters*, **61**(17), P. 3605–3607 (2007).

[20] Wang Y.Q., Yuan S.L., Liu L., et al. Ferromagnetism in Fe-doped ZnO bulk samples. *J. Magnet. Magnetic Mater.*, **320**(8), P. 1423–1426 (2008).

[21] Wang Y.Q., Cheng X.R., Su L., et al. The structure and magnetic properties of $Zn_{0.99}Fe_{0.01}O$ synthesized under high pressure. *Solid State Commun.*, **152**(7), P. 581–584 (2012).

[22] Krasil'nikov V.N., Gyrdasova O.I., Buldakova L.Y., et al. Synthesis and Photocatalytic Properties of Highly Dispersed Zinc Oxide Doped with Iron. *Doklady Chemistry*, **437**(2), P. 496–498 (2011).

[23] Zhukov V.P., Krasil'nikov V.N., Perelyaeva L.A., et al. Electronic Band Structure and Optical Absorption of Nanotubular Zinc Oxide Doped with Iron, Cobalt, or Copper. *Phys. Solid State*, **55**(12), P. 2331–2339 (2013).

[24] Krasil'nikov V.N., Gyrdasova O.I., Buldakova L.Y., Yanchenko M.Y. Synthesis and Photocatalytic Properties of Low-Dimensional Cobalt-Doped Zinc Oxide with Different Crystal Shapes. *Russ. J. Inorg. Chem.*, **56**(2), P. 145–151 (2011).

[25] Gyrdasova O.I., Krasil'nikov V.N.., Shalaeva E.V., et al. Synthesis and Structure of Quasi-One-Dimensional Zinc Oxide Doped with Manganese. *Russ. J. Inorg. Chem.*, **57**(1), P. 72–78 (2012).

[26] Gyrdasova O.I., Krasil'nikov V.N., Melkozerova M.A., et al. Synthesis, Microstructure, and Native Defects of Photoactive $Zn_{1-x}Cu_xO$ Solid Solutions ($0 \leqslant x \leqslant 0.1$) with Tubular Aggregates. *Doklady Chemistry*, **447**(1), P. 258–261 (2011).

[27] Gyrdasova O.I., Melkozerova M.A., Krasil'nikov V.N., et al. Synthesis and Native Defectivity of $Zn_{1-x}V_xO$ ($0 \leqslant x \leqslant 0.03$) Photocatalysts. *Bull. Russ. Acad. Sci. Phys.*, **77**(3), P. 305–308 (2013).

[28] Melkozerova M.A., Krasil'nikov V.N., Gyrdasova O.I., et al. Effect of Doping with 3d Elements (Co, Ni, Cu) on the Intrinsic Defect Structure and Photocatalytic Properties of Nanostructured ZnO with Tubular Morphology of Aggregates. *Phys. Solid State*, **55**(12), P. 2340–2345 (2013).

[29] Gyrdasova O.I., Krasil'nikov V.N., Shalaeva E.V., et al. Optical and Photocatalytic Properties of Quasi-One-Dimensional ZnO Activated by Carbon. *Mendeleev Commun.*, **24**, P. 143–144 (2014).